# Tectono-magmatic, sedimentary and hydrothermal history of Arsinoes and Pyrrhae Chaos, Mars

**Erica Luzzi[1], Angelo Pio Rossi[1], Cristian Carli[2] and Francesca Altieri[2]**

[1]Jacobs University, Bremen, Germany

[2]Inaf-IAPS Tor Vergata, Rome, Italy

Corresponding author: Erica Luzzi (e-luzzi@jacobs-university.de)

## Key points

- We produced a geomorphic map of Arsinoes and Pyrrhae Chaos, including the graben/fissures occurring throughout the study area;
- Spectral analyses of the light-toned deposits provide clues for sedimentary and hydrothermal minerals; spectral analyses of the bedrock are indicative of basaltic compositions;
- The observed volcano-tectonic surface features suggest a piecemeal caldera collapse as a possible mechanism of formation for the chaotic terrains.

**Abstract**

Arsinoes and Pyrrhae Chaos are two adjacent chaotic terrains located east to Valles Marineris and west to Arabia Terra, on Mars. In this work we produced a morpho-stratigraphic map of the area, characterized by a volcanic bedrock disrupted into polygonal mesas and knobs (Chaotic Terrain Unit) and two non-disrupted units interpreted as sedimentary and presenting a spectral variation, likely associated to hydrated minerals. The reconstructed geological history of the area starts with the collapse that caused the formation of the chaotic terrains. Since volcano-tectonic evidences are widespread all-over the area (e.g. fissure vents/graben, radial and concentric systems of faults, y-shaped conjunctions, lava flows, pit chains), and an intricate system of lava conduits is hypothesized for the occurrence of such features, we propose the possibility that the whole collapse was caused primarily by volcano-tectonic processes. On Earth, polygonal blocks and systems of concentric + radial fissures are originated in the frame of a particular caldera collapse called *chaotic* or *piecemeal*. In the study area on Mars, the chaotic collapse would have been triggered by repeated inflation and deflation of a putative magma chamber in depth under the terrain. In a late stage, after the end of the volcano-tectonic activity, a lacustrine/evaporitic depositional environment could have set, with the deposition of the non-disrupted units. The hydrated minerals found in the periphery of the Chaos could be the result of hydrothermal alteration of the basaltic bedrock.

*Keywords:Chaotic terrains; Caldera collapse; Mapping; Spectral analyses; Mars; Hydrothermal system.*

**Plain Language Summary**

Chaotic terrains are peculiar features on Mars. They consist of broad regions characterized by a variable surface disruption pattern of large polygonal blocks. Proposed generic scenarios in the literature always included a collapse, possibly caused by a range of processes (magma-ice interactions, melting of buried ice, groundwater pressure, etc.). In this work, we propose a new mechanism of formation for closed Chaotic terrains: a caldera collapse. The evidences supporting our hypothesis include the volcano-tectonic assemblage found within the terrain. Additionally, our mineralogical analyses suggest that during a late stage of the volcanic activity a hydrothermal system could have set. In such scenario hot water would have risen from the subsurface through fractures created by the volcanic activity, evolving from explosive to hydrothermal. The detection of possible new hydrothermally-generated deposits bears potential also for the search of past evidences of life.

# 1 Introduction

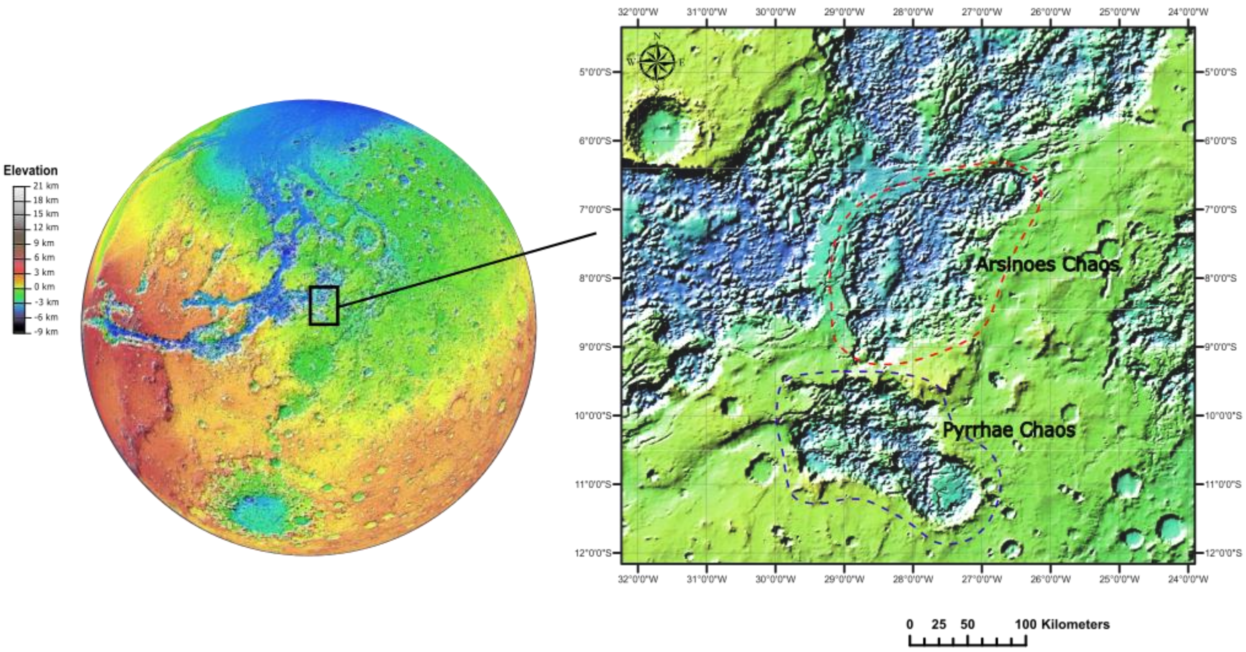


Fig. 1: Location of Arsinoes and Pyrrhae Chaos on a MOLA Global Color Shaded Relief.

Arsinoes and Pyrrhae Chaos are two adjacent Chaotic terrains, respectively centered at 7.8°S, 332°E and 10.3°S, 331.5°E (Fig. 1), a few tens of kilometres south of Aureum Chaos and a few hundred kilometres SW of Aram Chaos, sharing with the latter many structural and depositional characteristics. Several mechanisms of formation were proposed in literature to explain the nature of the putative collapse responsible for the disruption of the bedrock into polygonal blocks that characterizes the chaotic terrains. The proposed scenarios include: i) a major role played by groundwater and cryosphere, particularly linked to changes of pressure within the aquifer that caused the disruption of the bedrock and subsequent water outflow (Andrews-Hanna & Phillips, 2007; Carr, 1979; Harrison & Grimm, 2009; Rodriguez et al., 2005), ii) the occurrence of a buried ice lake that after melting would have caused fracturing and catastrophic outflow (Manker & Johnson, 1982; Roda *et a*l., 2014; Zegers *et al*., 2010), iii) catastrophic destabilization of buried clathrates (Hoffman, 2000; Kargel et al., 2007), and iv) magma-cryosphere/groundwater interactions (Chapman & Tanaka, 2002; Head & Wilson, 2007; Leask *et al*., 2006; Meresse et al., 2008; Wilson & Head III, 2002). Given the complexity of the current geologic setting of Arsinoes and Pyrrhae Chaos, possibly augmented by several million years of erosion and mantling, a possible interaction between the proposed processes (or singular contributions at different times) must also be considered.

In the present work we performed geomorphic and stratigraphic mapping of Arsinoes and Pyrrhae Chaos and a spectral analysis of the deposits; in addition, we propose a possible sequence of events to explain the occurrence of the collapsed bedrock (involving an early caldera collapse) and the sedimentary units (involving a later-stage aqueous depositional environment).

## 1.2 Regional setting

The first comprehensive description of the Chaotic terrains was made by Sharp et al. (1971) using Mariner 6 imagery, followed by Sharp (1973) based on Mariner 9 data and Schultz et al. (1982) based on Viking data. In this early stage of research, the main features of Martian Chaotic terrains were already clear and these areas were defined as deeply collapsed terrains disrupted into an irregular pattern of tilted mesas and knobs, in some cases associated with outflow channels. The Chaotic Terrain Unit was first defined by Schultz and Rogers (1982) and then with a refinement by Glotch & Christensen (2005) into three subunits: Fractured Plains, Knobby Terrain and High Thermal Inertia Chaotic Terrain. The Chaotic Terrain Unit represents the basaltic bedrock over a large area including several other Chaotic terrains such as Aureum, Aram, Hydratoes, Aurorae, Chryse and Hydaspis Chaos. The age of the Chaotic Terrain Unit according to Tanaka *et al.*, (2014) is Middle Noachian, with younger Hesperian ages in the internal portions of collapsed areas. With the collection of new compositional data from THEMIS (Thermal Emission Imaging System), TES (Thermal Emission Spectrometer), OMEGA (Observatoire pour la Minéralogie, l'Eau, les Glaces et l'Activité) and CRISM (Compact Reconnaissance Imaging Spectrometer for Mars), the investigations in literature focused mainly on the sedimentary units lying on top of the basaltic bedrock. Several authors analyzed the mineralogy of the layered sedimentary units occurring for example in Aram Chaos (Catling & Moore, 2003; P. R. Christensen *et al*., 2001; Dobrea *et al*., 2008; Gendrin *et al*., 2005; Timothy D Glotch & Christensen, 2005; Lichtenberg *et al*., 2010; Liu *et al.*, 2012; Massé *et al.*, 2008; Ormö *et al*., 2004), Aureum and Iani Chaos Chaos (Dobrea *et al.*, 2008; Glotch & Rogers, 2007). Hematite deposits associated with monohydrated and polyhydrated sulfates were spatially correlated with layered sedimentary units, separated by an unconformity from the basaltic bedrock. The occurrence of hydrated sulfates and hematite led the previously cited authors to assume that an aqueous and/or hydrothermal depositional environment must have set after the collapse of the bedrock. The sedimentary layered deposits in Arsinoes Chaos were not included in the previous studies, while in Pyrrhae Chaos the sedimentary deposits are not observed at all. The lack of studies in this location emphasizes the need to expand our knowledge of this area, providing a broader context on Martian Chaotic terrains.

# 2 Data and methods

## 2.1 Data, processing and tools

The imagery used to perform the geological mapping were provided by the CTX (Context Camera)(Malin *et al.*, 2007) and HiRISE (High Resolution Imaging Science Experiment)(McEwen *et al*., 2007) instruments onboard the MRO (Mars Reconnaissance Orbiter). One HRSC (High Resolution Stereo Camera, on board Mars Express spacecraft) image was also used to observe in false colour the study area and one HRSC DEM was downloaded for the contours in eastern Pyrrhae Chaos, since the area is not covered by CTX stereo pairs. CTX imagery was used as a basemap; in particular we used a global blended CTX mosaic provided by the Murray Lab (Dickson *et al*., 2018). HiRISE images were used to observe in detail the stratigraphic contacts in certain areas: EDR products were processed and tiled through the USGS software ISIS3 (Gaddis *et al.*, 1997). The data processing was supported by GNU Parallel (Tange, 2011). Changes in thermal inertia were investigated on JMARS (Java Mission-planning and Analysis for Remote Sensing)(Christensen *et al*., 2009) developed by ASU's Mars Space Flight Facility. JMARS is a GIS-system where different layers can be loaded on a global basemap: it was used to visualize the THEMIS (Thermal Emission Imaging System) night-time infrared.

DEMs from CTX were computed using ASP (Ames Stereo Pipeline) developed by NASA (Beyer *et al.*, 2018; Moratto *et al.*, 2010): the resulting products are bundle-adjusted to the global topography (MOLA - Mars Orbiter Laser Altimeter). A list of the used images is provided in Table 1.

| Dataset | Image ID | Stereo pair |
|---|---|---|
| **HiRISE** | ESP_016658_1735 | - |
| **HiRISE** | ESP_020060_1715 | - |
| **HiRISE** | ESP_026996_1725 | - |
| **HiRISE** | ESP_027629_1730 | - |
| **HiRISE** | ESP_034499_1710 | - |
| **HiRISE** | ESP_035356_1715 | - |
| **HiRISE** | ESP_036622_1720 | - |
| **HiRISE** | ESP_037545_1730 | - |
| **HiRISE** | ESP_039352_1730 | - |
| **HiRISE** | ESP_053883_1730 | - |
| **HiRISE** | PSP_002180_1720 | - |
| **CTX** | B05_011700_1720_XI_08S028W | B06_012056_1721_XI_07S028W |
| **CTX** | F10_039563_1729_XN_07S027W | P04_002747_1736_XN_06S027W |
| **CRISM** | frt00008233_07 | - |
| **CRISM** | frt00023790_07 | - |
| **CRISM** | frt000196b0_07 | - |
| **HRSC** | h1947_0000 | - |
| **HRSC** | h1958_0000 | |

Table 1: ID of the data used for this work.

The imagery was then imported into ESRI Arcgis for the geological mapping. The attitudes were measured using the beta version of LayerTools (Kneissl *et al.*, 2011), kindly provided by Dr. Thomas Kneissl.

The CRISM (Murchie *et al.*, 2007) cubes (*S* detector - short wavelength channel, and *L* detector - long wavelength detector) with full resolution (FRT) available in the study area (also listed in Table 1) were processed by means of the software ENVI (with the CAT extension) where atmospheric corrections and projection were applied, allowing the subsequent visualization and analysis of the spectra.

## 2.2 Mapping

### 2.2.1 Scale

The geological map of the area (Fig. 10) was digitized on ArcGIS at the CTX resolution (~5 m/px), but the chosen output scale is 1:3.000.000. At first, the standard approach suggested by Tanaka *et al.*, (2009) was considered:

$$So_n = S_m \times n$$

Where $So_n$ is the output scale, $S_m$ is the raster resolution x 2000 and $n$ is the factor between the digitizing scale and the output scale (the authors suggest a number between 2 and 5). Using this criteria and considering $n = 5$ to get the best resolution for the small mapped deposits, in this case the resulting output scale would have been 1:50.000, while a smaller scale was required for a proper visualization; therefore this approach was abandoned.

Only craters with a diameter larger than 2 km were mapped.

### 2.2.2 Polygonal features – Geomorphic units

The geomorphic units observed in the study area are five and were mapped as polygons. The units include the three subunits of the Chaotic Terrain unit (*Fractured Plains*, *Knobby Terrain* and *High Thermal Inertia Chaotic Terrain*) and the non-disrupted units (*Light-toned Layered Unit* and *Cap unit*). Furthermore, the inner part of the post-collapse craters was mapped as an additional unit: *Post Collapse Craters*. Following the USGS guideline (2005), we chose warm colours for the Chaotic Terrain subunits given their volcanic nature. On the other hand we chose to use cold colours for the non-disrupted units since they were interpreted as sedimentary deposits and green for the craters so that they could be clearly distinguished from the bedrock.

### 2.2.3 Linear features – Structural features and contacts

The mapped linear features include the crater rims, the contacts between different units and the structural features. The fractures affecting the bedrock and the elongated graben-like depressions were included in a single category called *Graben/fissures*. This choice is mainly due to the coalescence of the structures and the difficulty in distinguishing them. The second group of structural features is represented by the wrinkle ridges. The contacts were divided into *certain* contacts (continuous lines) and *approximate/inferred* contacts (dotted lines), for those cases where the mantling covers the contact (e.g. between Cap Unit and Light-toned Layered Unit) or if the change from one unit to another is transitional (e.g. between Knobby Terrain and High Thermal Inertia Chaotic Terrain).

### 2.2.4 Surface features – Pit chains and pitted areas

Pit chains and diffuse pits are widespread throughout the study area. In several parts the high density of pits did not allow to map the single pit chains, leading to the necessity to introduce a polygonal feature to indicate these areas (*Pitted areas*).

### 2.2.5 Symbols

The symbology used for crater rims, graben, pit chains, wrinkle ridges, certain and approximate contacts was chosen in agreement with the standards recommended by USGS and FGDC for planetary mapping. For pitted areas we introduced a new symbol. All the symbols are listed in the legend of Fig. 13.

## 3 Results

### 3.1 Morphological observations and stratigraphy

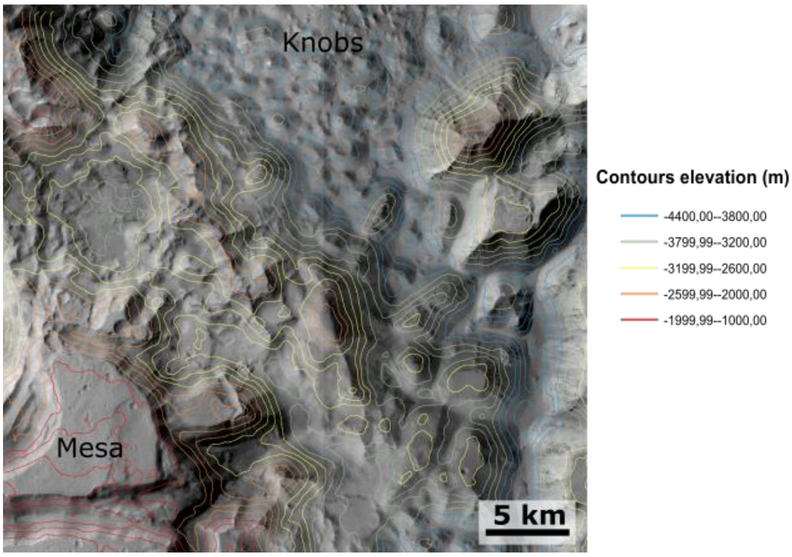


Figure 2: Elevation contours in Pyrrhae Chaos showing the mesas of the Fractured plains at higher elevations compared the mounds of the Knobby Terrain. CTX mosaic; HRSC DEM from orbit *h1958_0000*.

The oldest unit observed in Arsinoes and Pyrrhae Chaos is the Chaotic Terrain Unit, composed by three subunits: Fractured Plains (characterized my angular flat-topped blocks), the Knobby Terrain (displaying rounded mounds) and the High Thermal Inertia Chaotic Terrain (heavily eroded and characterised by the higher thermal inertia). The Fractured Plains are predominantly occurring along the rim of the Chaos, while the Knobby Terrain acts as a transition towards the inner parts of the Chaos. The Knobby Terrain subunit is the most extensive material representing the Chaotic Terrain Unit in this area. The Knobby Terrain is in contact with the sharp angular mesas of the Fractured Plains (Fig. 2) and the small mounds of the High Thermal Inertia Chaotic Terrain, even though the latter occurs only in a small area in the NE part of Arsinoes Chaos and seems not to be present in Pyrrhae Chaos. The rounded mounds characterizing the Knobby Terrain are located at lower elevations compared to the mesas of the Fractured Plains (Fig. 2). The faults bounding the mesas of the Fractured Plains show a depth up to 1 km and the flat-topped blocks appear as irregular polygonal bodies. Stratigraphically above the Chaotic Terrain Unit, non-disrupted and layered deposits lie unconformably. In Arsinoes Chaos, the non-disrupted deposits overlying the Chaotic Terrain Unit displays two different morphologies and attitude-based domains. Furthermore, they occur at different elevations showing their stratigraphic relationship. Therefore, they were considered as two separated units (Fig. 3). At lower elevations light-toned deposits are characterized by planar bedding and scalloped surfaces; their aspect resembles the ILDs (Interior Layered Deposits) described by Sowe *et al*. (2007), Le Deit *et al.* (2008) and Schmidt *et al*. (2018). The average attitude of the light-toned layered deposits is ~100.20 (dip direction.dip angle). The light-toned layered unit fills the voids between the mounds of the Knobby Terrain (Fig. 4), assuming often a lobate shape and wrapping around the knobs. The overlying sedimentary deposits are separated from the light-toned layered deposits by an unconformity: the attitude of the youngest deposits (informally called Cap Unit due to the fact that these deposits “seal” the succession) is ~290.03. The Cap Unit does not seem to be layered or if it is, the bedding is massive and the outcrop visible today represents only one thick bed with a plateau-like aspect. The occurrence of the non-disrupted units only in certain areas of the Chaos leads to question whether the current extent represents approximately the original extent or the erosion obliterated a large portion of the deposits that were originally covering the entire Chaos.

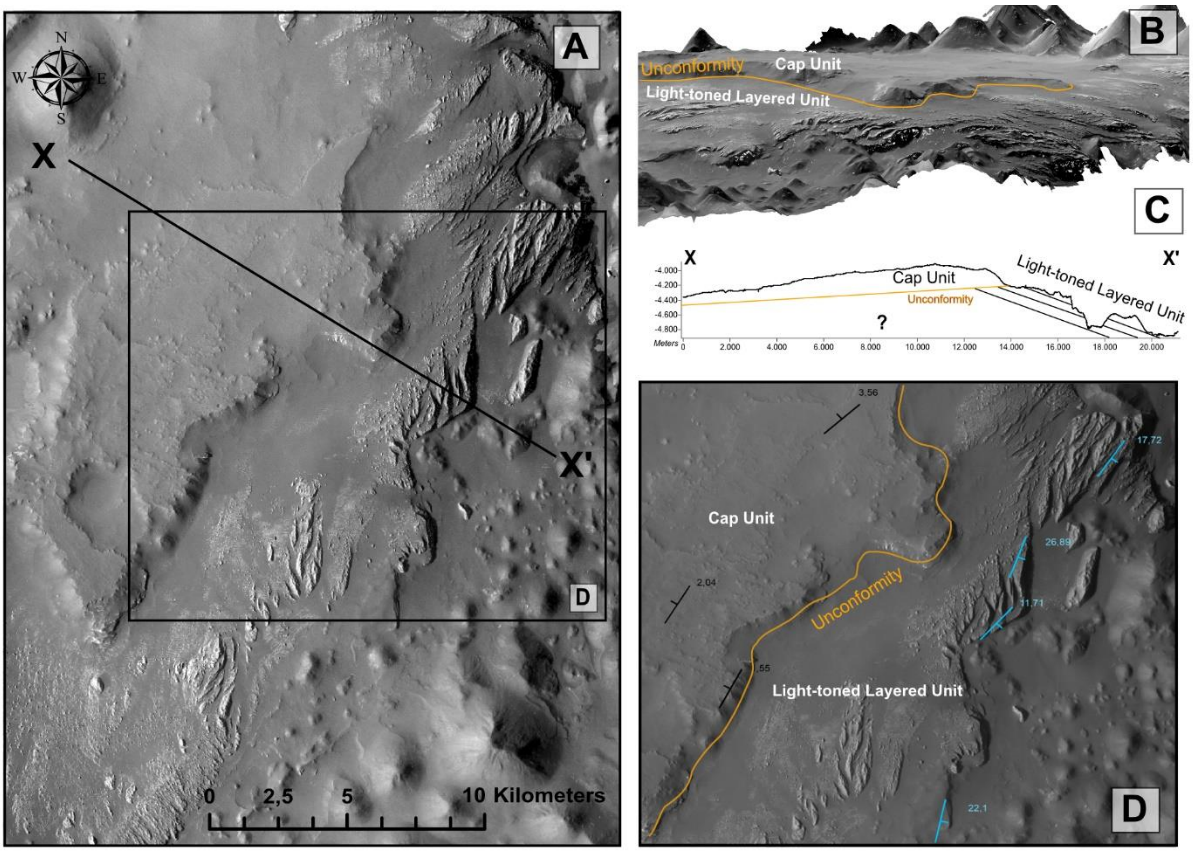


Figure 3: A) Overview map of the area where the contact between the two non-disrupted units occurs. The black square bounds the area depicted in D. The section X-X' refers to the topographic profile in C. B) 3D view of the stratigraphic contact between the Light-toned Layered Unit and the Cap Unit, separated by the unconformity (in blue). C) Topographic profile showing the plateau-like morphology of the Cap Unit and the different attitude of the units. D) Some of the attitudes measured with LayerTools (light blue: Light-toned Layered Unit; black: Cap Unit). CTX stereo pair: *B05_011700_1720_XI_08S028W* and *B06_012056_1721_XI_07S028W*.

In Pyrrhae Chaos the non-disrupted sedimentary units are not present, although the two adjacent Chaos show a similar depth (in certain areas of Pyrrhae Chaos the depth is even higher than Arsinoes Chaos).

### 3.2 Structural observations

In Arsinoes and Pyrrhae Chaos, as well as in other Chaotic terrains, the main structural feature is represented by the deep fractures bounding the polygonal blocks of the Fractured Plains. The nature of these fractures is mainly dilational. The minimum depth of the

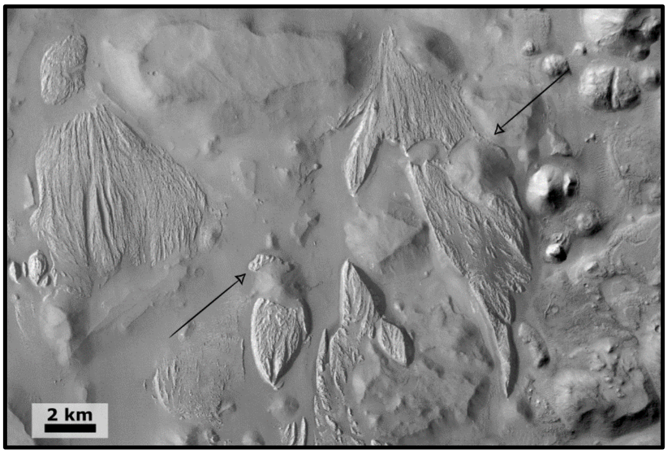


Figure 4: The light-toned layered deposits overlying the Knobby Terrain and outflanking the mounds (black arrows). The superposition relationships suggest a younger age of the layered deposits relatively to the knobs. Note also the tendency to assume a lobate morphology. CTX: *F10 039563 1729 XN 07S027W*.

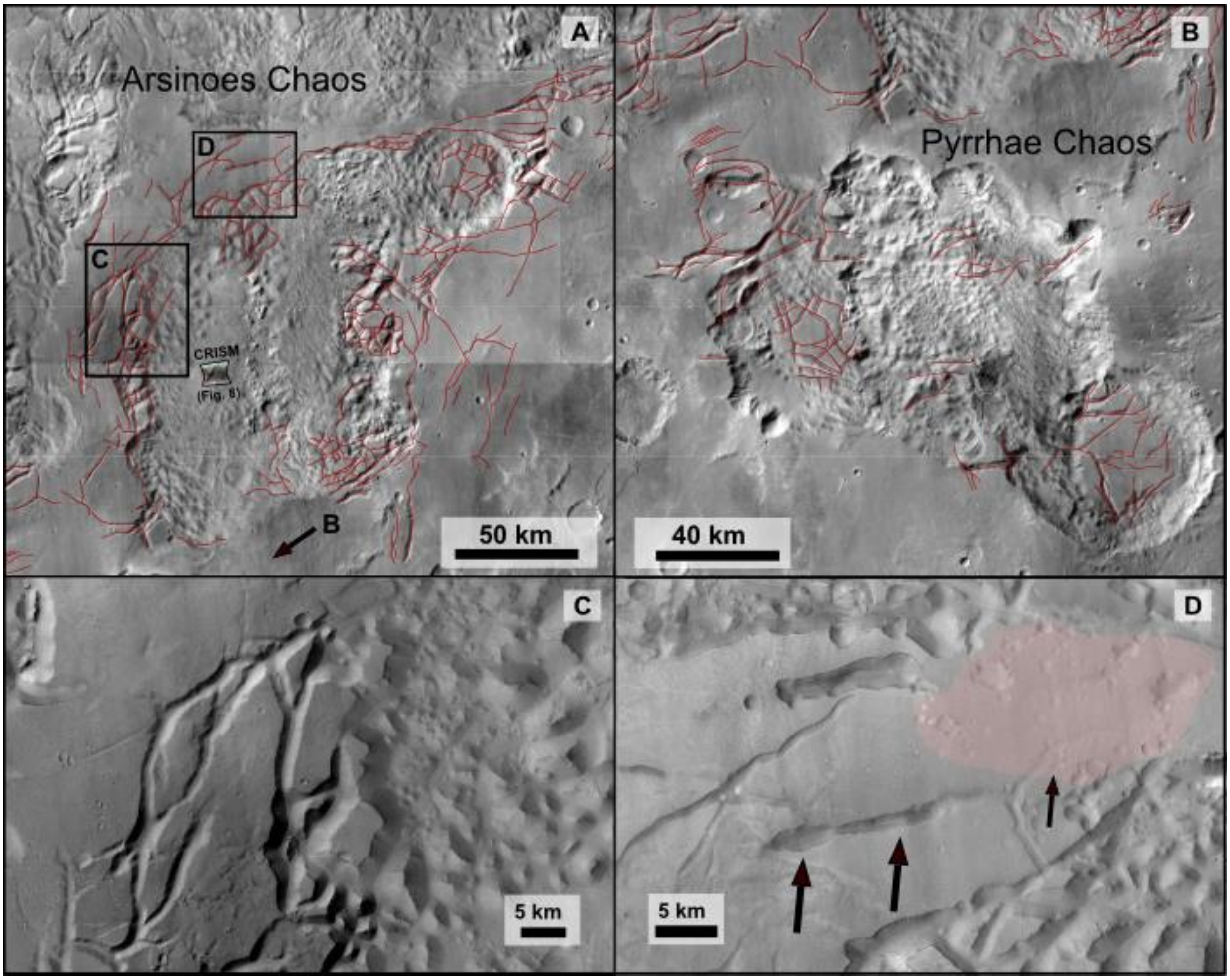


Figure 5: The faults and the elongated graben-like depressions are mapped in red in Arsinoes Chaos (A) and Pyrrhae Chaos (B). Not that in 5A the location of Fig. 5 B-C-D and Fig. 7 is indicated. C) The elongated graben-like depressions occur close to the faults affecting the Fractured Plains and it is difficult to distinguish their separation. D) The elongated graben-like depressions are also coalescent with pit chain (black arrows) and are often associated with heavily pitted areas (pink area). CTX mosaic.

fractures can be assumed by the height of the mesa from the floor, and it is on the order of few hundred meters, up to 1 km. Additionally, it is common that the floor of the Chaotic terrain accommodates non-disrupted units, thus forbidding to observe the real depth of the blocks. The orientation of fractures bounding the blocks follows two trends that show variations throughout the chaos. The polygonal geometries are due to the irregularly orthogonal disposition of these two trends (Fig. 5a-b).

A large number of elongated graben-like depressions was mapped (Fig. 5a-b). These confined structures that may resemble channels at a first glance, are often in coalescence with the orthogonal fractures of the polygonal mesas (Fig. 5c). In addition, the elongated graben-like depressions are also in coalescence with pit chains and/or occur in areas heavily pitted (Fig. 5d). Considering graben-like depressions and fractures as belonging to the same group of structures, two patterns can be distinguished based on their orientation: one group of structures seems to follow the rim of the Chaos, showing a concentric pattern; another group shows instead a radial pattern. When these two sets cross each other, polygonal blocks are defined. The elongated graben-like depressions have a linear or slightly sinuous morphology and do not show any braided system nor meanders. The depth range is between 100 and 400 meters, while the length can reach up to 40 km. Moreover, several elongated graben-like depressions display y-shaped bifurcations and in some cases they are associated with lava flows (e.g. south-eastern

Pyrrhae Chaos, Fig.6a). The lava flow in Pyrrhae Chaos has a darker tone compared to the surroundings in the HRSC false colour image. In addition, the lava flow shows higher thermal inertia than the surrounding materials in the THEMIS night-time infrared (Fig. 6b).

Although the non-disrupted deposits do not have complete lateral continuity, no major faults affecting them were detected, not even at the HiRISE resolution. However, due to the lack of continuity of these deposits for the erosion, we can’t exclude at all the existence of younger faults affecting the layered deposits that have been eroded.

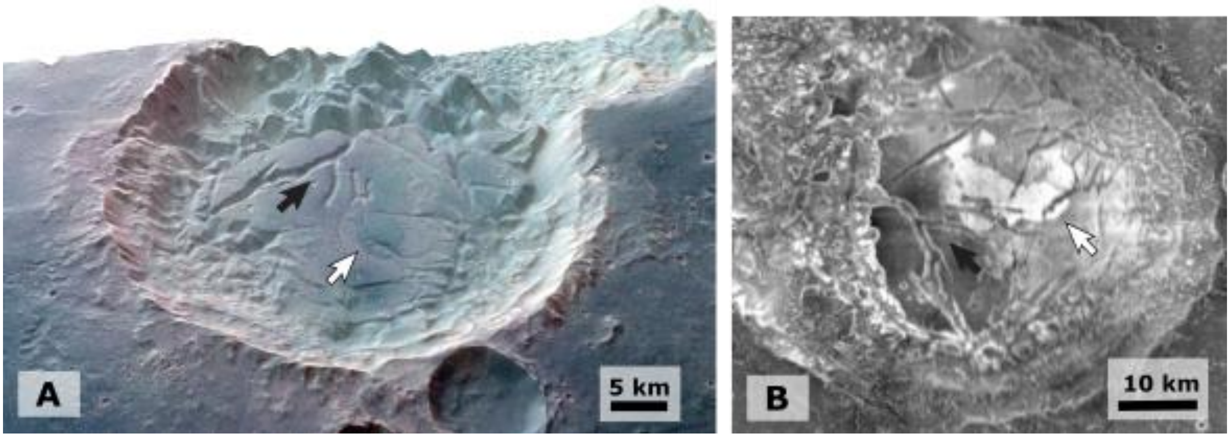


Figure 6: A) 3D view of the false colour HRSC image *h1947_0000*, showing a difference in tone between the Fractured Plains materials and the lava flow pointed out by the white arrow. The black arrow points a y-shaped conjunction within an elongated graben-like depression in the south-eastern Pyrrhae Chaos. B) The same features displayed in A are now showed in another perspective and in THEMIS night-time infrared. Note that the lava flow occurring in Pyrrhae Chaos (white arrow) has a thermal inertia higher than the surrounding materials.

Compressive structures such as wrinkle ridges were also observed ~30 km SE from Arsinoes Chaos (Fig. 7), providing an important clue on the existence of a compressional regional stress. The wrinkle ridges show a typical orientation ~N-S and are characterized by sinuous/arcuate morphologies.

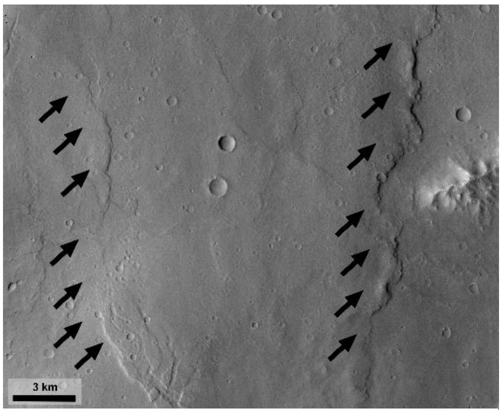


Figure 7: Two wrinkle ridges are indicated by the black arrows. CTX mosaic.

The last important structural observation concerns the craters: two major pre-collapse craters were incorporated in the collapse in the periphery of the study area, one in the north-eastern Arsinoes Chaos and one in the south-eastern Pyrrhae Chaos (depicted in Fig. 6). The embodying of the craters within the collapse was likely due to the reactivation of pre-existing weaknesses caused by the impacts.

### 3.3 Thermal Inertia

The surface temperature of a given area depends on the properties of the exposed materials but it is also affected by external factors such as dust covering and atmospheric pressure. Diurnal changes in temperature can be detected and described through the thermal inertia, a bulk property of materials defined by the relationship between thermal conductivity, density and specific heat of the considered material. These properties are different for each material and some of the factors influencing the thermal behaviour are for example grain size, eventual cementation, packaging of the grains and degree of exposure. Therefore surfaces with different thermal inertia are most likely indicative of a change in composition and/or physical properties. A material with high thermal inertia is able to gather the heat and conduct it beneath the surface during the day, while during the night the stored heat is released through the surface (Mellon *et al*., 2000). In this way the surface appears cold during the day and warmer during the night. High thermal inertia is typical of consolidated/lithified, such as an exposed bedrock, lava flows, indurated and compact rocks; on the other hand unconsolidated sands and dust show a low thermal inertia (Fergason *et al*., 2006). On Mars, thermal information are provided by TES (Thermal Emission Spectrometer, see e.g. Jakosky *et al.*, 2000; Christensen *et al.*, 2001), on board Mars Global Surveyor, and THEMIS (Thermal Emission Imaging System, see e.g. Philip R. Christensen *et al*., 2004), on board 2001 Mars Odissey. We investigated the thermal inertia visualising the THEMIS nigh-time infrared on JMars. As anticipated in the previous sections, two areas with higher thermal inertia were identified in the study area. The first area occurs in Arsinoes Chaos and corresponds to the most eroded part of the Chaotic Terrain Unit that was identified as the High Thermal Inertia Chaotic Terrain subunit. The differentiation from the Knobby Terrain is transitional and was complicated to delineate a sharp boundary, but the high thermal inertia seems to coincide with the most eroded and peaked knobs, completely lacking flat surfaces where the mantling could find accommodation space. The second area is located in Pyrrhae Chaos and corresponds to a lava flow (Fig. 6). In this case the contrast is sharp and well-defined, despite the lava flow occurs on a flat surface that could host a substantial amount of dust. In the same area other small regions show high thermal inertia, coinciding with the margin of the mesas and the steep slopes.

### 3.4 CRISM spectral analyses

In the nearby Aram Chaos, Glotch & Christensen (2005), detected mixtures of sulfates and phyllosilicates (associated with plagioclases and pyroxenes) in different percentage in all the non-disrupted units (Cap Unit and layered units), using the TES and THEMIS datasets. Part of the layered deposits was interpreted by the authors as hematite-bearing, while within other layered deposits the iron oxide was not found. Moreover, Lichtenberg *et al.* (2010) provided a stratigraphic and mineralogical characterization of the hydrated sulfates occurring in Aram Chaos, based on CRISM data. The authors identified two sedimentary units: the oldest consisting of monohydrated sulfates intercalated with ferric hydroxy-sulfate or nanophase ferric oxides and the youngest bearing polyhydrated sulfates and crystalline hematite. Monohydrated sulfates were detected by Lichtenberg *et al.* (2010) observing minor absorptions at 2.1 and 2.4 μm; ferric hydroxy-sulfate was interpreted through absorptions at 2.238 μm, associated with minor absorptions at 1.49, 1.82, and 2.38 μm; polyhydrated sulfates were inferred from the absorptions at 1.9 and 2.4 μm within the youngest unit unconformably lying on the oldest with monohydrated sulfates. Polyhydrated sulfates in association with crystalline gray hematite have been found also by Dobrea *et al*. (2008) in Aram, Aureum and Iani Chaos: using the TES and OMEGA datasets, the authors were able to point out a correlation between all these Chaotic terrains East to Valles Marineris. Sowe *et al.* (2012) analysed CRISM spectra from Aureum Chaos, and also in this case the authors were able to identify within the light-toned layered units hydroxylated, monohydrated, polyhydrated sulfates. The hydroxylated sulfates were interpreted by the authors based on the absorptions at 2.23 μm (related to the occurrence of OH), 1.42–1.45 μm and its weak 1.93 and 2.4 μm bands. Monohydrated sulfates (kieserite) were detected through absorptions at 2.12 μm and a major absorption at 2.4 μm, while polyhydrated sulfates were diagnosed based on absorptions at 1.42–1.44 and at 1.92–1.93 μm.

Considering these evidences from the nearby Aram and Aureum Chaos and given the morphologic analogies, we investigate if similar mineralogies can be detected also in Arsinoes Chaos.

Within the inner region of Arsinoes Chaos only one full resolution CRISM cube is available (*frt00008233_07_if164*). This cube was analysed in order to characterize the non-disrupted units overlying the basaltic bedrock. A first distinction of spectrally different terrains was made based on the RGB images (Fig. 8) with combined summary products (Viviano-Beck *et al*., 2014). These products were preliminarily considered taking into account the minerals revealed by previous works on Chaotic terrains. In Fig. 8C the summary parameter for chlorides shows a possible occurrence of hydrated minerals (in yellow). The putative hydrated minerals coincide in extent with the morphologically identified Light-toned Layered Unit. The RGB composites derived from the parameters that are specifically used to identify hydrated minerals (such as sulfates and phyllosilicates) did not provide a clear distinction of a mineralogical variation. Moreover, the difficulty in finding a spectrum with clear evidences of hydrated minerals is attributed to the detection limit and to the noise affecting the data. Therefore, summary products suggest a mineralogical variation and likely bearing hydrated minerals, but the spectra do not allow the detection of specific minerals. The interpretation of these deposits as sedimentary can only be supported by analogies with the adjacent chaotic terrains and by the morpho-stratigraphic observations.

Other hydrated minerals were found in the northeastern periphery of Arsinoes Chaos (CRISM cube *frt000196b0_07*), in correspondence of some of the collapse features previously described. In this area (shown in Fig. 9), at the boundary with Aureum Chaos, also analyses on the bedrock were performed (CRISM cube *frt00023790_07* and *frt000196b0_07*).

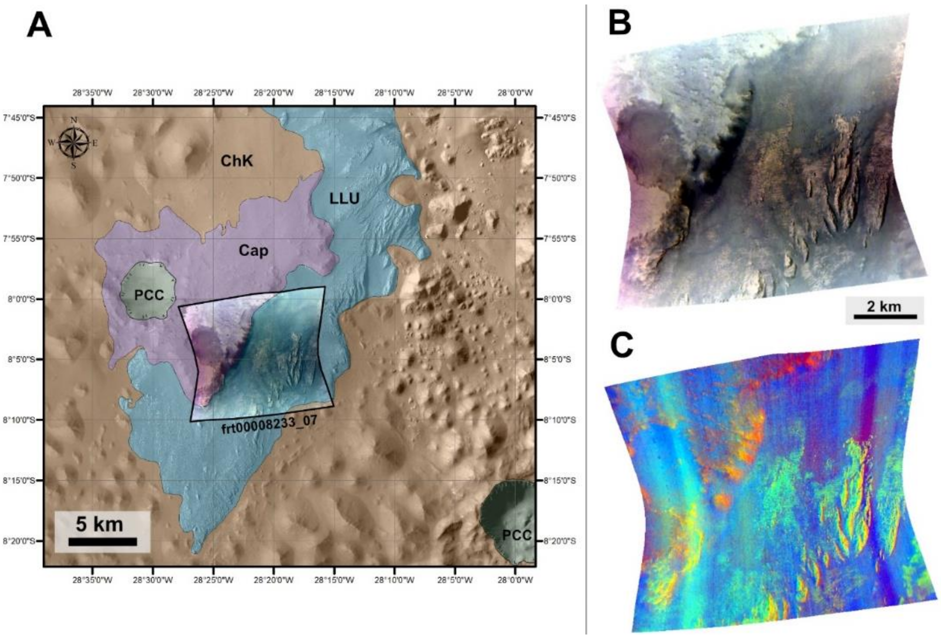


Figure 8: **A)** Location of the CRISM *cube frt00008233_07* superposed on the geomorphic map where the different units are shown. The complete geomorphic map with legend is presented in Fig. 10. **B)** True colors image (R=R600; G=R530; B=R440). **C)** RGB composite with summary parameters of the CRISM TRDR *frt00008233* scene. CHL: Chlorides are in blue, yellow/green are indicative of hydrated minerals (R= ISLOPE; G= BD3000; B=IRR2).

The hydrated minerals detected in the CRISM cube *frt000196b0_07* are concentrated in the central area of the cube, precisely coinciding in extent with an exhumated deposit slightly different in albedo from the surrounding materials. As shown in Fig. 10A, a mineralogical variation is already distinguishable from the infrared false color image where the hydrated minerals appear to be pale green. This first clue is therefore additionally supported by the RGB composites in Fig. 10B and 10C. In 10B the RGB composite PFM is shown for the detection of Fe and Mg in the crystalline structure of the hydrated phyllosilicates, in particular for significant band depths at 2.3 μm; as a result, Fe-Mg hydrated phyllosilicates are displayed as cyan, allowing to appreciate the mineralogical variation at a first glance. For the ratioed spectrum the numerator is an average of some of the cyan pixels shown in Fig. 10B having both band depth at 1.9 and 2.3 micron well above the detection limit, while the denominator is an average of pixels with relatively flat spectra picked from the same column of their respective numerators. The resulting ratioed spectrum is reported in Fig. 10, where a comparison with spectra from the CRISM resampled library is provided. Several phyllosilicates sharing similar absorptions (indicative of Fe,Mg-OH) were plotted in order to compare even the weakest absorption to understand the corresponding mineral that may occur in the deposit. We interpreted the ratioed spectrum as smectite, since the ratioed spectrum and the smectite's spectrum share the same absorptions, including the absorption at 2.28 μm that is instead shifted toward > 2.3 μm in the other plotted phyllosilicates, due to a bigger concentration of Fe instead of Mg (Clark *et al.*, 1990).

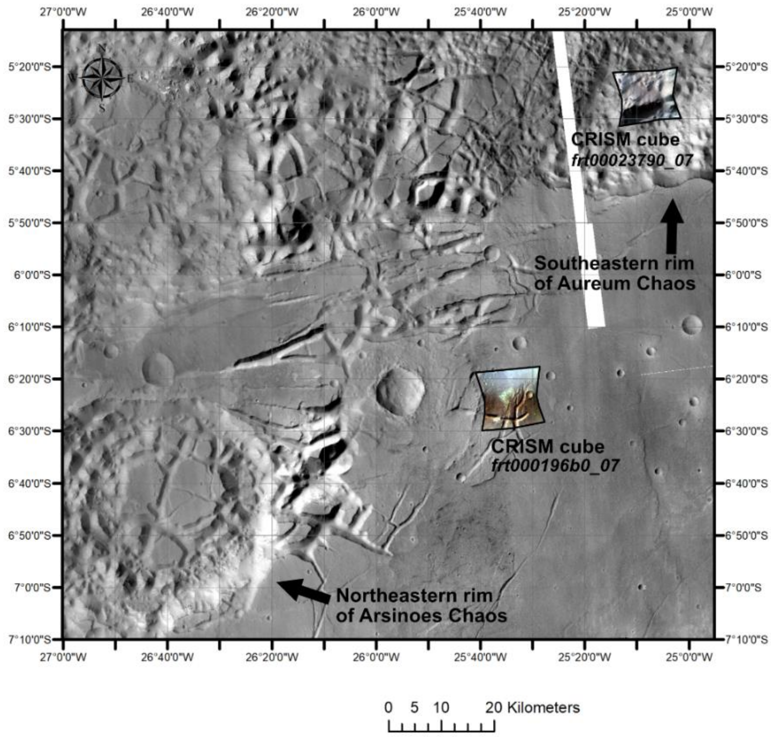


Figure 9: Location of the peripheral CRISM cubes *frt00023790_07 and frt000196b0_07* on the CTX mosaic.

On the same CRISM cube *frt000196b0_07* analyses of the bedrock revealed the occurrence of mafic minerals, in particular pyroxenes with low Ca content. A first identification of the pyroxenes was made by analyzing the summary product LCPINDEX2 (low-Ca pyroxenes) (Fig. 11). A significant spectrum for the analysis of the bedrock results from the CRISM cube *frt00023790_07*, where broad absorptions at 1 μm and 2 μm confirm the occurrence of pyroxenes (Fig. 12) (Viviano-Beck *et al*., 2014). The asymmetry of the absorption at 1 μm towards longer wavelength could also be associated with the occurrence of a second mafic phase as olivine or an high-Ca pyroxene, with variations in breadth due to the amount of Fe and Mg or Ca (Cloutis *et al*., 1986; King & Ridley, 1987). Pyroxenes and olivine are indicative of basaltic compositions. This observation supports the basaltic nature of the bedrock of the Chaotic terrain (Chaotic Terrain Unit).

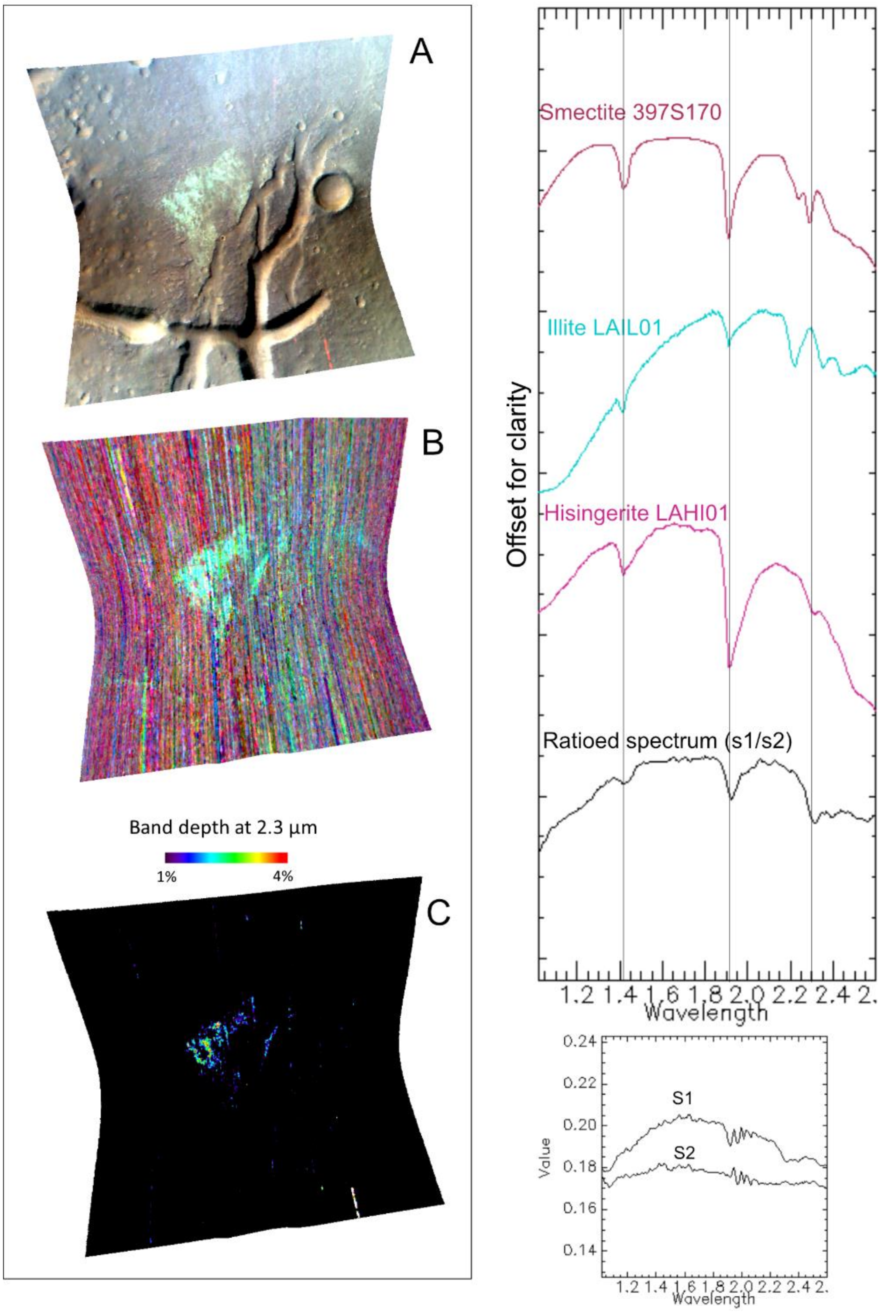


Figure 10: A) Infrared false color scene showing a mineralogical variation between the exhumed deposits and the surrounding bedrock. B) RGB composite with summary products for phyllosilicates with Fe and Mg (PFM: cyan colors, coinciding with the albedo variation, indicate Fe/Mg smectites, R=BD2355; G=D2300; B=BD2290). C) The band depth at 2.3 μm is significant in correspondence of the hydrated minerals. On the right the ratioed spectrum is compared to resampled CRISM spectra of Smectite 397S170, Illite LAIL01, and Hisingerite LAHI01 from the spectral library. The black lines highlight the absorptions of the ratioed spectrum at 1.42, 1.92 and 2.28 μm.
CRISM cube *frt000196b0_07.*

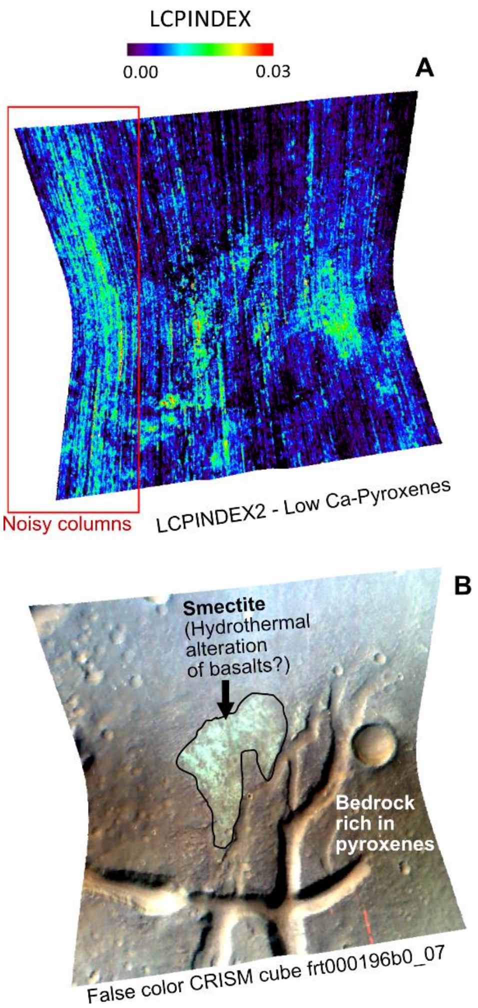


Figure 11: A) LCPINDEX shows the abundances of pyroxenes on the bedrock. B) Interpretation of the mineralogical variation: in the central region the hydrated minerals are interpreted as Fe-Mg phyllosilicates (smectite), while the bedrock rich in pyroxenes is indicative of basaltic compositions.
CRISM cube *frt000196b0_07*

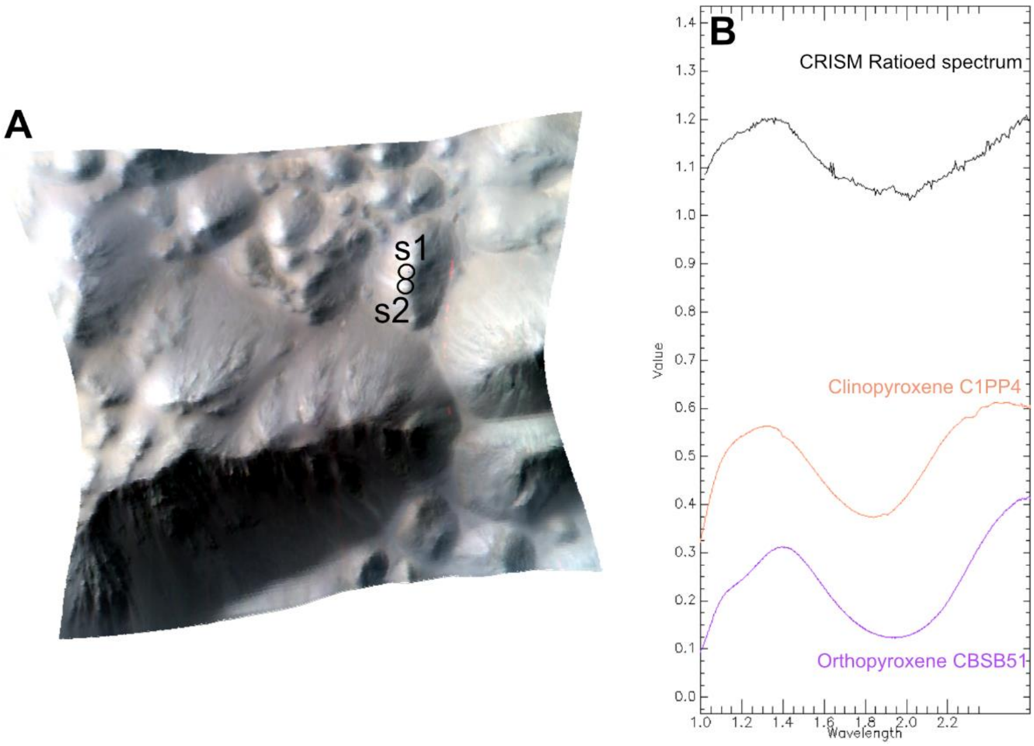


Figure 12: A) false color scene and location of s1 and s2; B) the ratioed spectrum is compared to the CRISM resampled spectra for clinopyroxene C1PP4 and orthopyroxene CBSB51. Both the absorption at 1 µm and the broad absorption at 2 µm are present and consistent with a mafic composition. CRISM cube *frt00023790_07*.

### 3.5 Morpho-stratigraphic map

Based on the observations carried on and described in the previous section, a geomorphic map of the area was produced (Fig. 13).

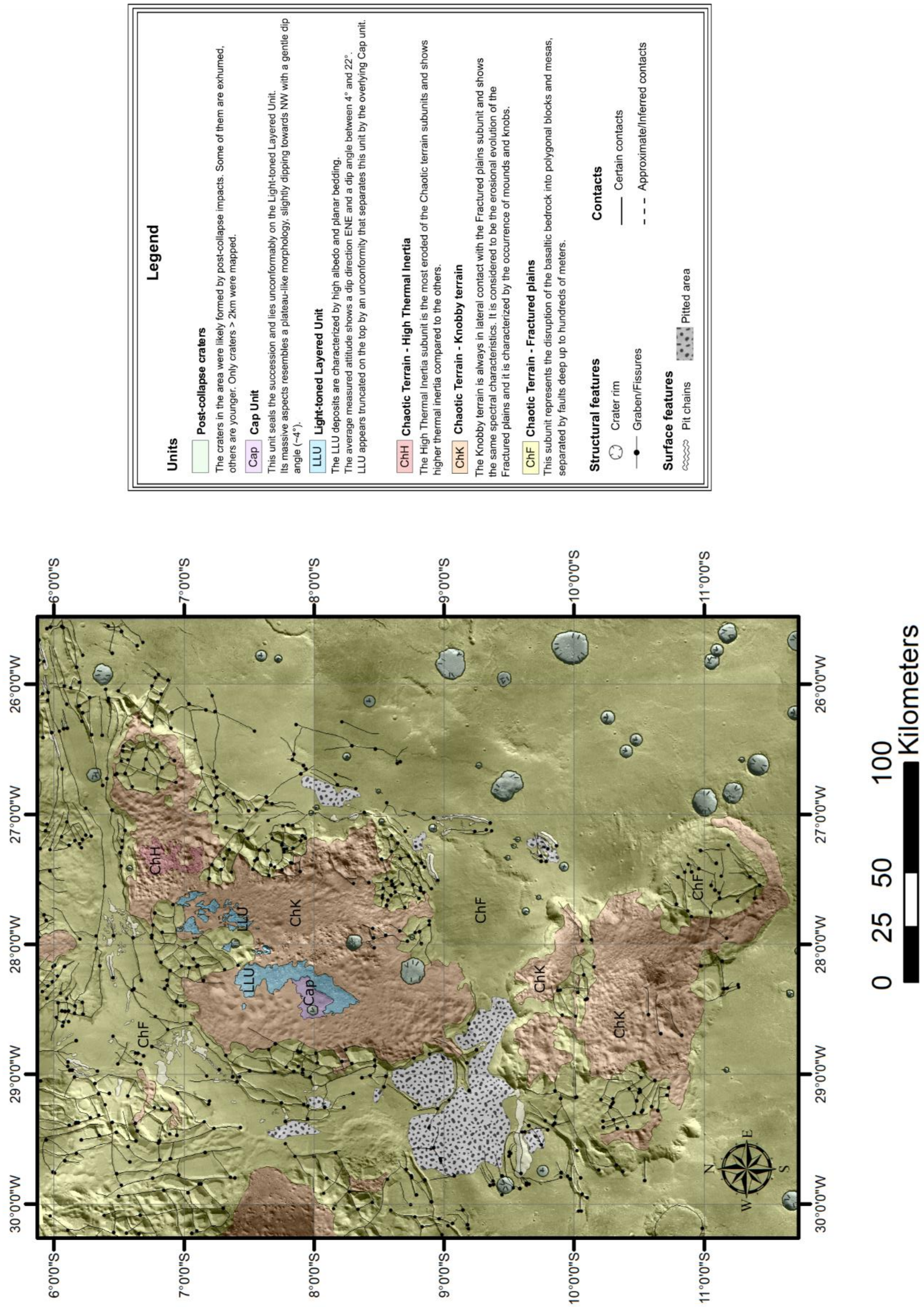


Figure 13: Morpho-stratigraphic map of Arsinoes and Pyrrhae Chaos.

# 4 Discussion

## 4.1 Bedrock collapse

The widespread occurrence of the elongated graben-like depressions leads to question their nature in the frame of the investigation about the origin of the collapse. From here onwards this kind of structures will be called informally *fissure* or *graben*, with no reference to the pure extensional regime that is normally associated with grabens on Earth. Similar structures within the Tharsis region, on Olympus Mons and Ascraeus Mons, were already interpreted as fissure vents by Mouginis-Mark & Christensen (2005). In first instance, we rule out the possibility that the fissures may have any connection with fluvial systems: no braided nor meandering patterns were recognized, as well as no typical fluvial depositional morphologies anywhere in the study area. Since outflow channels are lacking, a volcano-tectonic origin seems more likely, considering the basaltic mineralogies all-over the area, the presence of y-shaped conjunctions indicative of inflation and at least one evident lava flow in correspondence of the fissures. Therefore, these grabens may be considered as the result of the collapse of lava conduits or eruptive fissures or both. Another surface evidence for such collapses may be represented by the extensive pits and pit chains, that at a first glance may resemble small craters but lack in ejecta and raised rims. Pits and pit chains were interpreted in literature as the surface collapse of buried conduits or as the result of explosive activity, likely due to interactions between magma and $H_2O$ (Head & Wilson, 2002; Wyrick *et al.*, 2004).

Another interpretation based on a terrestrial analogue was proposed by Ferrill *et al.* (2011), who observed pit chains in Iceland formed by the interplay of dilational faults, extension fractures, and tectonic caves. The authors suggested a similar combination of mechanisms for the formation of pit chains on Mars. In our study area, pits and pit chains are often coalescent with grabens, suggesting extremely unstable conditions. The fact that most of the dilational orthogonal fractures bounding the polygonal blocks and accommodating the deformation, interrupt on the rim while outward the grabens are mostly concentric, parallel to the *ring fault*, recalls a geological process known on Earth as chaotic caldera collapse, caused by repeated cycles of inflation and deflation of a magma chamber overlying the area.

Troll *et al.* (2002) performed an analogue experiment to test the hypothesis that the collapse of the Tejeda caldera (Canary Islands) was due to multicycle processes of inflation and deflation of the magma chamber. The result of the experiment, where an inflated and deflated balloon has been placed below a certain volume of sands, shows radial and concentric patterns of faults that generate polygonal blocks arranged chaotically and that interrupt mostly on the ring fault. This type of caldera collapse is also called *piecemeal* or *noncoherent* and has been studied on Earth by several authors (Scandone, 1990; Branney & Kokelaar, 1994; Moore & Kokelaar, 1998; Roche *et al*., 2000; Walter & Troll, 2001; Troll *et al.* 2002). Unlike the piston calderas, where a nondeformed area (piston) is surrounded by tilted strata, in the chaotic collapse the piston is disrupted during the subsidence, generating a breakup of the floor into blocks with a chaotic arrangement. According to Roche *et al.* (2000), the existence of a regional stress may act as a catalyst of the process. We compared the results of the analogic experiment of Troll *et al.* (2002) with Arsinoes and Pyrrhae Chaos and from the morphological point of view the association of concentric and radial faults with polygonal blocks seems to be consistent with the hypothesis of a piecemeal caldera collapse. The geometry of the calderas is in both cases circa elliptical, but both in Arsinoes and Pyrrhae Chaos the imbedding of ancient impact craters makes the geometry of the caldera more complex.

The structural weakness of the impact craters was likely facilitating the inclusion of these disrupted areas in the collapse, that can reactivate pre-existing faults due to the impact. The role played by ancient impact craters in the formation of chaotic terrains has been investigated by several authors (Carr, 1979; Rotto & Tanaka, 1995; Rodriguez *et al.*, 2005) who consider the structural control of the impact craters a crucial contribute together with surface extensional fabrics. The regional stress invoked by Roche *et al.* (2000) as an enhancing factor may be represented in Arsinoes and Pyrrhae Chaos by the compressional regime testified by the wrinkle ridges identified in the region between and adjacent the two chaotic terrains.

Furthermore, on Mars, collapsed depressions previously believed to be impact craters were interpreted by Michalski & Bleacher (2013) as *supervolcanoes*, namely volcanic constructs ("plains-style caldera complexes") not necessarily associated with major edifices but able to produce huge volumes of magma in the past. Thus, the hypothesis of a collapsed caldera has been already considered for depressed areas on Mars, but never for Chaotic terrains. Furthermore, features similar to the fissures that abound in Arsinoes and Pyrrhae Chaos were mapped and interpreted as vents in Ascraeus Mons (Mars) by Pozzobon *et al.* (2015). Such vents would have erupted lavas coming from a complex network of dykes, while collapse pits would be associated with feeder dykes. Pozzobon *et al.* (2015) investigated the distribution of the vents in terms of fractal clustering, obtaining as a result a possible depth of the magma chamber. The same approach may be used in future for Arsinoes and Pyrrhae Chaos, determining: i) if the occurrence of a magma chamber in depth is reasonable based on the distribution of the fractures, and ii) an estimate of possible ranges of depth.

Since the grabens occur also in peripheral areas, a complex plumbing system is assumed to radiate from the putative magma chamber, affecting thus the surface not uniquely within the single Chaos.

The high thermal inertia of the lava flow occurring in Pyrrhae Chaos suggests that this lava flow is younger than the surrounding bedrock. In fact the high thermal inertia is normally observed in lava flows, but the fact that the basaltic bedrock does not show high thermal inertia (except for the most eroded subunit, the High Thermal Inertia Chaotic Terrain and for the steep slopes of the mesas) is due to the fact that the Chaotic Terrain unit must be older than the overlying lava flow, therefore more affected by mantling and weathering, while the lava flow is still acting thermally as a rocky surface. The interplay between dust cover and thermal behaviour has been already investigated on Mars by Crown & Ramsey (2017), based on a THEMIS IR survey in Arsia Mons. The authors describe the difficulties in discriminating the effect of mantling and albedo from the real thermal inertia, but they were able to identify two types of lava flow: one group with relatively high albedo and large extent and a second one darker, smooth and smaller, associated with elongated channels and fissures, very similar to the lava flow observed in Pyrrhae Chaos.

On steep slopes and sharp knobs there is no stability nor accommodation space for the dust; therefore it is reasonable to infer that the higher thermal inertia is related to the better exposition of the bedrock. On the other hand, the flat top of the mesa where the lava flow occurs, should host dust. At this point the contrast of thermal inertia may not be due to different accommodation spaces and repose angles, but perhaps on the time of exposition to the mantling. Assuming that the lava flow is younger than the bedrock means that it would have suffered for a shorter time span the action of weathering and mantling. The age of the lava flow may thus coincide with the age of the volcanic activity that caused the collapse of the oldest basaltic bedrock or it could testify a late reactivation.

A sketch to show the proposed chaotic caldera collapse is provided in Fig. 14 (1), where multiple cycles of inflation and deflation of the magma chamber result in the collapse accompanied by concentric and radial faults polygonal blocks. A pervasive network of buried faults and lava conduits contributes to the coalescence of the collapses and in some cases the lava reaches the surface producing a lava flow.

### 4.2 Non-disrupted units

The Light-toned Layered Unit and the Cap Unit were interpreted as sedimentary deposits first of all for analogy with the nearby chaotic terrains, where deposits sharing the same characteristics of those in Arsinoes Chaos were already interpreted as sedimentary units and spectral analyses were already carried on (Dobrea *et al*., 2008; Glotch *et al*., 2005; Glotch & Christensen, 2005; Glotch & Rogers, 2007; Lichtenberg *et al*., 2010; Sowe *et al*., 2012). Furthermore, we interpreted the non-disrupted units as sedimentary for the following reasons:

- Lack of volcano-tectonic features;
- High albedo;
- Planar bedding;
- More prone to erosion than the surrounding basalts.
- Mineralogical variation that could be associated with occurrence of hydrated minerals

The reason why the NIR absorption features are not as prominent as in other CRISM data from Aureum and Aram Chaos may be due to several factors: a minor abundance of the hydrated minerals, absence of areas bereft of hydrated minerals within the CRISM cube (thus the denominator cannot be ideal), lack of totally dust-free areas, features below the detection limit. Especially for the Cap Unit, it was not possible to speculate from a compositional point of view about the presence of hydrated silicates indicated in other similar sedimentary units because even in the RGB with combined summary products no significant variation was appreciable.

Nevertheless, the observed variation in the Light-toned Layered Unit could be consistent with the interpretation of the layered deposits in the adjacent Chaotic terrains, except for the high concentration of hematite that was well described in Aram and Aureum Chaos but was not found in Arsinoes Chaos. The hematite in Aram Chaos is considered by Glotch & Christensen (2005) as a fundamental key for a lacustrine interpretation together with the bedding, the close geometry of the basin and the outflow channels. Despite the lack of hematite (missing or simply below the detection limit) and the outflow channels in Arsinoes Chaos the hypothesis of a lake or evaporitic basin as a depositional environment for the Light-toned Layered Unit cannot be excluded either. We consider reasonable that a closed and deep basin such as Arsinoes Chaos, that seems to possibly host hydrated minerals, might have been filled by groundwater after the caldera collapse.

It remains uncertain why in Pyrrhae Chaos the succession stops at the Chaotic Terrain Unit. The depth of the basin is approximately the same as Arsinoes Chaos (even deeper) and their proximity would suggest that the same processes should have acted, but for some reason the deposition of sedimentary units after the collapse did not happen in Pyrrhae Chaos (or the deposits were completely eroded).

The exhumed light-toned deposit found in the north-eastern periphery of Arsinoes Chaos were instead interpreted as related to hydrothermal activity that could have set as soon as the volcanic activity responsible of the collapse has begun to stabilize. This hypothesis is supported by the evidence of smectite within the deposit. In this case, the hydrated minerals are not in a close basin, but in correspondence of the volcano-tectonic structures that we interpreted as directly related to volcanic collapses. Furthermore, the associations of basaltic minerals (pyroxenes) and hydrated Fe-Mg phyllosilicates (smectite) can be explained by a process of hydrothermal alteration, as summarized by Inoue (1995). According to the author, smectite can be the result of hydrothermal alteration of andesitic to basaltic compositions under neutral or alkaline conditions.

On Earth, this has been observed in several geological contexts, including stagnant hydrothermal alteration of caldera deposits (Inoue *et al*., 1984). The extent of the hydrothermal deposit is limited to 1.3 km and for scale reasons it was not possible to include it in the geomorphic map. Nevertheless, in the surrounding area light-toned exhumed patches are visible, suggesting an extent of the hydrothermal deposit of at least 10 km.

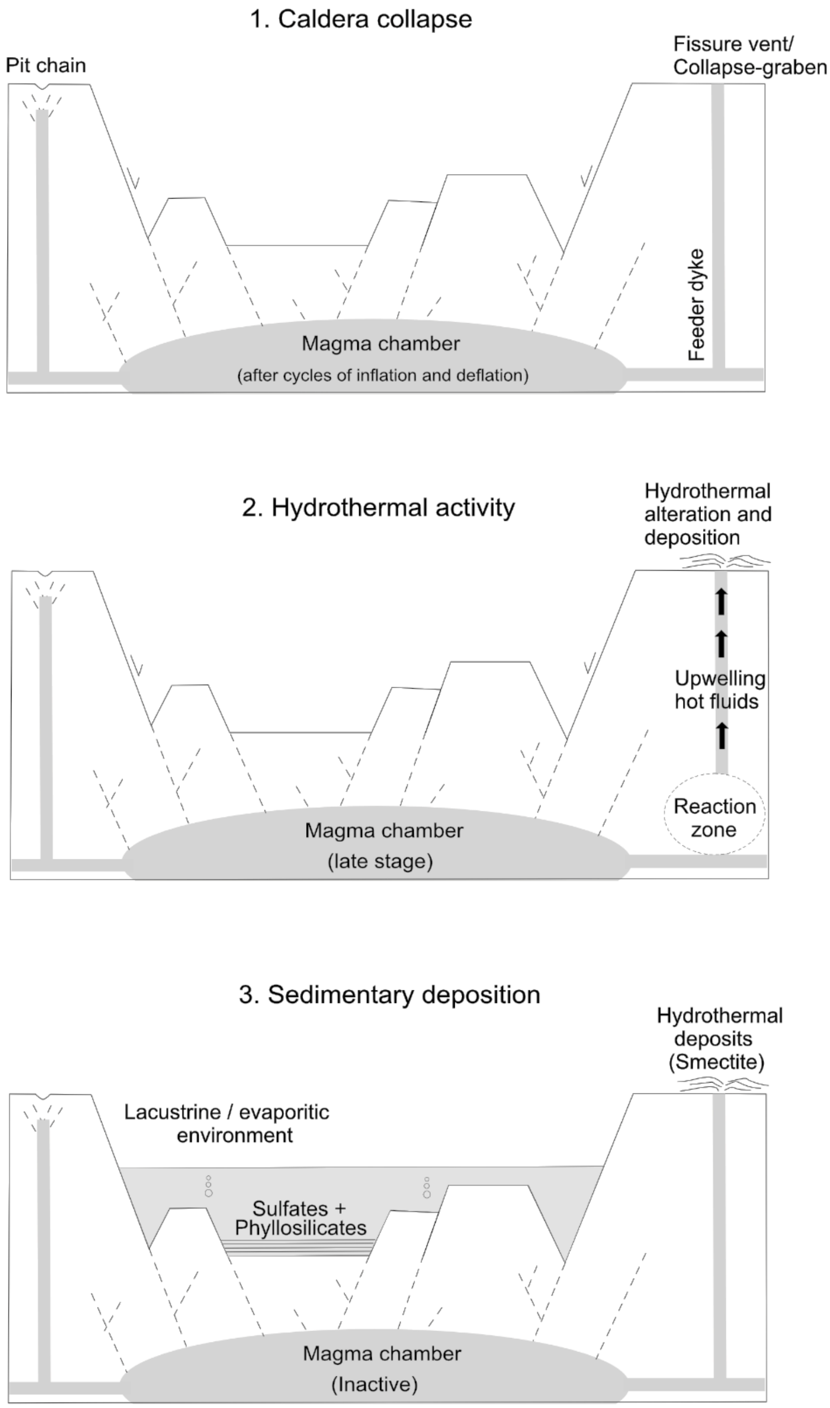


Figure 14: The interpretation of the geological history of Arsinoes and Pyrrhae Chaos is represented in this sketch through 3 stages. 1) Chaotic caldera collapse after multiple cycles of inflation and deflation of the magma chamber. 2) Late volcanic activity with generation of the hydrothermal system. 3) Arsinoes Chaos is filled by water and the sedimentary units are deposited unconformably on the bedrock.

## 5 Conclusion

The morpho-stratigraphic mapping performed in Arsinoes Chaos highlighted the occurrence of two major groups of geomorphic units: the Chaotic Terrain, further divided into three subunits (Fractured Plain, Knobby Terrain and High Thermal Inertia Chaotic Terrain) represents the bedrock of the area and it is characterized by polygonal irregular mesas and rounded knobs;

the second group is composed by two non-disrupted units that were deposited after the collapse of the Chaotic Terrain and lie unconformably on top of the bedrock.

The Light-toned Layered Unit is characterized by a planar bedding and the scalloped surfaces show high albedo; the Cap Unit seems instead to be a single thick layer (plateau-like) and lies unconformably on top of the Light-toned Layered Unit. In Pyrrhae Chaos the non-disrupted units are missing.

The spectral analyses performed in Arsinoes Chaos could not entirely confirm the morpho-stratigraphic evidences of the sedimentary deposits with the presence of hydrated phase similar to the case of Aram and Aureum lying on the bedrock of the Chaotic Terrain Unit. Nevertheless a mineralogical variation is present and the existence of hydrated minerals below CRISM detection limits cannot be ruled out.

The bedrock was characterized as basaltic in composition due to the occurrence of mafic minerals, in particular low-Ca pyroxenes; the CRISM analyses did not reveal crucial information on the Cap Unit and Light-toned Layered Unit, but the detection of hydrated minerals hosted by a small deposit located in proximity of the collapse-related structure in the northeastern periphery of Arsinoes Chaos was possible and we detected hydrated Fe-Mg phyllosilicates (likely smectite). While the Light-toned Layered Unit may be explained by a lacustrine/evaporitic environment that could have been established after the caldera collapse and the stabilization of the volcanic activity, the hydrated minerals occurring in the northeastern periphery cannot be explained by such a hypothesis because they are not placed into a close basin, but they drape the volcano-tectonic structures interpreted as collapse graben and/or fissure vents. For this reason the most likely hypothesis involves a hydrothermal system where hot water rises through the fractures, deposits hydrated minerals and alters the pre-existing basaltic bedrock. The structural evidences of volcano-tectonic activity support this interpretation, suggesting that after the caldera collapse a residual volcanic activity may have turned into a hydrothermal environment warming up the groundwater that was infiltrating the fractures and finally reaching the surface with processes of deposition and alteration. The geological history of the area is summarized in Fig.14.

Further investigations will elaborate the chaotic caldera collapse applied to this case of study through numerical, analogic and 3D modelling.

## 6 Acknowledgments

We acknowledge support and funding from the European Union's Horizon 2020 research and innovation programme under grant agreement Nº776276 (PLANMAP).

## 7 References

Andrews-Hanna, J. C., & Phillips, R. J. (2007). Hydrological modeling of outflow channels and chaos regions on Mars. *Journal of Geophysical Research: Planets*, *112*(E8).

Beyer, R. A., Alexandrov, O., & McMichael, S. (2018). The Ames Stereo Pipeline: NASA's Open Source Software for Deriving and Processing Terrain Data. *Earth and Space Science*, *5*(9), 537–548. https://doi.org/10.1029/2018EA000409

BRANNEY, M. J., & KOKELAAR, P. (1994). Volcanotectonic faulting, soft-state deformation, and rheomorphism of tuffs during development of a piecemeal caldera, English Lake District. *Geological Society of America Bulletin*, *106*(4), 507–530. https://doi.org/10.1130/0016-

7606(1994)106<0507:VFSSDA>2.3.CO;2

Carr, M. H. (1979). Formation of Martian flood features by release of water from confined aquifers. *Journal of Geophysical Research*, *84*(B6), 2995. https://doi.org/10.1029/JB084iB06p02995

Catling, D. C., & Moore, J. M. (2003). The nature of coarse-grained crystalline hematite and its implications for the early environment of Mars. *Icarus*, *165*(2), 277–300. https://doi.org/10.1016/S0019-1035(03)00173-8

Chapman, M. G., & Tanaka, K. L. (2002). Related magma--ice interactions: Possible origins of chasmata, chaos, and surface materials in Xanthe, Margaritifer, and Meridiani Terrae, Mars. *Icarus*, *155*(2), 324–339.

Christensen, P. R., Engle, E., Anwar, S., Dickenshied, S., Noss, D., Gorelick, N., & Weiss-Malik, M. (2009). JMARS - A Planetary GIS. *American Geophysical Union, Fall Meeting 2009, Abstract Id.IN22A-06*. Retrieved from http://adsabs.harvard.edu/abs/2009AGUFMIN22A..06C

Christensen, P. R., Morris, R. V., Lane, M. D., Bandfield, J. L., & Malin, M. C. (2001). Global mapping of Martian hematite mineral deposits: Remnants of water-driven processes on early Mars. *Journal of Geophysical Research: Planets*, *106*(E10), 23873–23885. https://doi.org/10.1029/2000JE001415

Christensen, P R, Bandfield, J. L., Hamilton, V. E., Ruff, S. W., Kieffer, • H H, Titus, T. N., … Greenfield, M. (2001). Mars Global Surveyor Thermal Emission Spectrometer experiment: Investigation description and surface science results. In *JOURNAL OF GEOPHYSICAL RESEARCH* (Vol. 106). https://doi.org/10.1029/2000JE001370

Christensen, Philip R., Jakosky, B. M., Kieffer, H. H., Malin, M. C., McSween, Jr., H. Y., Nealson, K., … Ravine, M. (2004). The Thermal Emission Imaging System (THEMIS) for the Mars 2001 Odyssey Mission. *Space Science Reviews*, *110*(1/2), 85–130. https://doi.org/10.1023/B:SPAC.0000021008.16305.94

Clark, R. N., King, T. V. V., Klejwa, M., Swayze, G. A., & Vergo, N. (1990). High spectral resolution reflectance spectroscopy of minerals. *Journal of Geophysical Research*, *95*(B8). https://doi.org/10.1029/jb095ib08p12653

Cloutis, E. A., Gaffey, M. J., Jackowski, T. L., & Reed, K. L. (1986). Calibrations of phase abundance, composition, and particle size distribution for olivine-orthopyroxene mixtures from reflectance spectra. *Journal of Geophysical Research*, *91*(B11), 11641. https://doi.org/10.1029/jb091ib11p11641

Crown, D. A., & Ramsey, M. S. (2017). Morphologic and thermophysical characteristics of lava flows southwest of Arsia Mons, Mars. *Journal of Volcanology and Geothermal Research*, *342*, 13–28. https://doi.org/10.1016/J.JVOLGEORES.2016.07.008

Dickson, J., Kerber, L., Fassett, C., & Ehlmann, B. (2018). A Global, Blended CTX Mosaic of Mars With Vectorized Seam Mapping: A New Mosaicking Pipeline Using Principles of Non-Destructive Image Editing. *Lunar and Planetary Science Conference*.

Dobrea, E. Z. N., Poulet, F., & Malin, M. C. (2008). Correlations between hematite and sulfates in the chaotic terrain east of Valles Marineris. *Icarus*, *193*(2), 516–534.

Fergason, R. L., Christensen, P. R., & Kieffer, H. H. (2006). *High-resolution thermal inertia derived from the Thermal Emission Imaging System (THEMIS): Thermal model and applications*. https://doi.org/10.1029/2006JE002735

Ferrill, D. A., Wyrick, D. Y., & Smart, K. J. (2011). Coseismic, dilational-fault and extension-fracture related pit chain formation in Iceland: Analog for pit chains on Mars. *Lithosphere*, *3*(2), 133–142. https://doi.org/10.1130/L123.1

Gaddis, L., Anderson, J., Becker, K., Becker, T., Cook, D., Edwards, K., … Robinson, M. (1997). An Overview of the Integrated Software for Imaging Spectrometers (ISIS). *Lunar and Planetary Science Conference*, 387. Retrieved from https://ui.adsabs.harvard.edu/abs/1997LPI....28..387G/abstract

Gendrin, A., Mangold, N., Bibring, J.-P., Langevin, Y., Gondet, B., Poulet, F., … LeMouélic, S. (2005). Sulfates in Martian layered terrains: the OMEGA/Mars Express view. *Science (New York, N.Y.)*, *307*(5715), 1587–1591. https://doi.org/10.1126/science.1109087

Glotch, T D, Rogers, D., & Christensen, P. R. (2005). A newly discovered hematite-rich unit in Aureum Chaos: Comparison of hematite and associated units with those in Aram Chaos. *36th Annual Lunar and Planetary Science Conference*, *36*.

Glotch, Timothy D, & Christensen, P. R. (2005). Geologic and mineralogic mapping of Aram Chaos: Evidence for a water-rich history. *Journal of Geophysical Research: Planets*, *110*(E9).

Glotch, Timothy D, & Rogers, A. D. (2007). *Evidence for aqueous deposition of hematite- and sulfate-rich light-toned layered deposits in Aureum and Iani Chaos, Mars*. https://doi.org/10.1029/2006JE002863

Harrison, K. P., & Grimm, R. E. (2009). Regionally compartmented groundwater flow on Mars. *Journal of Geophysical Research: Planets*, *114*(E4).

Head, J. W., & Wilson, L. (2002). Mars: a review and synthesis of general environments and geological settings of magma-$H_2O$ interactions. *Geological Society, London, Special Publications*, *202*(1), 27–57. https://doi.org/10.1144/GSL.SP.2002.202.01.03

Head, J. W., & Wilson, L. (2007). Heat transfer in volcano–ice interactions on Mars: synthesis of environments and implications for processes and landforms. *Annals of Glaciology*, *45*, 1–13. https://doi.org/10.3189/172756407782282570

Hoffman, N. (2000). White Mars: A New Model for Mars' Surface and Atmosphere Based on CO2. *Icarus*, *146*(2), 326–342. https://doi.org/10.1006/ICAR.2000.6398

Inoue, A.; Utada, M.; Nagata, U.; Watanabe, T. (1984). Conversion of trioctahedral smectite to interstratified Chlorite/Smectite in Pliocene acidic pyroclastic sediments of the Ohyu district, Akita Prefecture, Japan. *Clay Science*, *6*(3), 103–116. https://doi.org/10.11362/jcssjclayscience1960.6.103

Inoue, A. (1995). Formation of Clay Minerals in Hydrothermal Environments. In *Origin and Mineralogy of Clays* (pp. 268–329). https://doi.org/10.1007/978-3-662-12648-6_7

Jakosky, B. M., Mellon, M. T., Kieffer, H. H., Christensen, P. R., Varnes, E. S., & Lee, S. W. (2000). The thermal inertia of Mars from the Mars Global Surveyor Thermal Emission Spectrometer. *Journal of Geophysical Research: Planets*, *105*(E4), 9643–9652. https://doi.org/10.1029/1999JE001088

Kargel, J. S., Furfaro, R., Prieto-Ballesteros, O., Rodriguez, J. A. P., Montgomery, D. R., Gillespie, A. R., … Wood, S. E. (2007). Martian hydrogeology sustained by thermally insulating gas and salt hydrates. *Geology*, *35*(11), 975–978.

King, T. V. V., & Ridley, W. I. (1987). Relation of the spectroscopic reflectance of olivine to mineral chemistry and some remote sensing implications. *Journal of Geophysical Research: Solid Earth*, *92*(B11), 11457–11469. https://doi.org/10.1029/JB092iB11p11457

Kneissl, T., Van Gasselt, S., Wendt, L., Gross, C., & Neukum, G. (2011). Layering and degradation of the Rupes Tenuis unit, Mars--a structural analysis south of Chasma Boreale. *Geological Society, London, Special Publications*, *356*(1), 257–279.

Le Deit, L., Le Mouélic, S., Bourgeois, O., Combe, J.-P., Mège, D., Sotin, C., … Bibring, J.-P.

(2008). Ferric oxides in East Candor Chasma, Valles Marineris (Mars) inferred from analysis of OMEGA/Mars Express data: Identification and geological interpretation. *Journal of Geophysical Research*, *113*(E7), E07001. https://doi.org/10.1029/2007JE002950

Leask, H. J., Wilson, L., & Mitchell, K. L. (2006). Formation of Aromatum Chaos, Mars: Morphological development as a result of volcano-ice interactions. *Journal of Geophysical Research: Planets*, *111*(E8).

Lichtenberg, K. A., Arvidson, R. E., Morris, R. V., Murchie, S. L., Bishop, J. L., Fernandez Remolar, D., … Roach, L. H. (2010). Stratigraphy of hydrated sulfates in the sedimentary deposits of Aram Chaos, Mars. *Journal of Geophysical Research*, *115*(E6), E00D17. https://doi.org/10.1029/2009JE003353

Liu, Y., Arvidson, R. E., Wolff, M. J., Mellon, M. T., Catalano, J. G., Wang, A., & Bishop, J. L. (2012). Lambert albedo retrieval and analyses over Aram Chaos from OMEGA hyperspectral imaging data. *J. Geophys. Res*, *117*, 0–11. https://doi.org/10.1029/2012JE004056

Malin, M. C., Bell, J. F., Cantor, B. A., Caplinger, M. A., Calvin, W. M., Clancy, R. T., … Wolff, M. J. (2007). Context Camera Investigation on board the Mars Reconnaissance Orbiter. *Journal of Geophysical Research: Planets*, *112*(E5).

Manker, J. P., & Johnson, A. P. (1982). Simulation of Martian chaotic terrain and outflow channels. *Icarus*, *51*(1), 121–132. https://doi.org/10.1016/0019-1035(82)90032-X

Massé, M., Mouélic, S. Le, Bourgeois, O., Combe, J.-P., Deit, L. Le, Sotin, C., … Langevin, Y. (2008). Mineralogical composition, structure, morphology, and geological history of Aram Chaos crater fill on Mars derived from OMEGA Mars Express data. *J. Geophys. Res*, *113*, 12006. https://doi.org/10.1029/2008JE003131

McEwen, A. S., Eliason, E. M., Bergstrom, J. W., Bridges, N. T., Hansen, C. J., Delamere, W. A., … Weitz, C. M. (2007). MRO's High Resolution Imaging Science Experiment (HiRISE). *Journal of Geophysical Research: Planets*, *112*(E5).

Mellon, M. T., Jakosky, B. M., Kieffer, H. H., & Christensen, P. R. (2000). High-Resolution Thermal Inertia Mapping from the Mars Global Surveyor Thermal Emission Spectrometer. *Icarus*, *148*, 437–455. https://doi.org/10.1006/icar.2000.6503

Meresse, S., Costard, F., Mangold, N., Masson, P., Neukum, G., & others. (2008). Formation and evolution of the chaotic terrains by subsidence and magmatism: Hydraotes Chaos, Mars. *Icarus*, *194*(2), 487–500.

Michalski, J. R., & Bleacher, J. E. (2013). Supervolcanoes within an ancient volcanic province in Arabia Terra, Mars. *Nature*, *502*(7469), 47.

Moore, I., & Kokelaar, P. (1998). Tectonically controlled piecemeal caldera collapse: A case study of Glencoe volcano, Scotland. *Geological Society of America Bulletin*, *110*(11), 1448. https://doi.org/10.1130/0016-7606(1998)110<1448:TCPCCA>2.3.CO;2

Moratto, Z. M., Broxton, M. J., Beyer, R. A., Lundy, M., & Husmann, K. (2010). Ames Stereo Pipeline, NASA's open source automated stereogrammetry software. *Lunar and Planetary Science Conference*, *41*, 2364.

Mouginis-Mark, P. J., & Christensen, P. R. (2005). New observations of volcanic features on Mars from the THEMIS instrument. *Journal of Geophysical Research: Planets*, *110*(E8).

Murchie, S., Arvidson, R., Bedini, P., Beisser, K., Bibring, J.-P., Bishop, J., … Wolff, M. (2007). Compact Reconnaissance Imaging Spectrometer for Mars (CRISM) on Mars Reconnaissance Orbiter (MRO). *Journal of Geophysical Research*, *112*(E5), E05S03. https://doi.org/10.1029/2006JE002682

Ormö, J., Komatsu, G., Chan, M. A., Beitler, B., & Parry, W. T. (2004). Geological features indicative of processes related to the hematite formation in Meridiani Planum and Aram Chaos, Mars: a comparison with diagenetic hematite deposits in southern Utah, USA. *Icarus*, *171*, 295–316. https://doi.org/10.1016/j.icarus.2004.06.001

Pozzobon, R., Mazzarini, F., Massironi, M., & Marinangeli, L. (2015). Self-similar clustering distribution of structural features on Ascraeus Mons (Mars): implications for magma chamber depth. *Geological Society, London, Special Publications*, *401*(1), 203–218.

Roche, O., Druitt, T. H., & Merle, O. (2000). Experimental study of caldera formation. *Journal of Geophysical Research: Solid Earth*, *105*(B1), 395–416.

Roda, M., Kleinhans, M. G., Zegers, T. E., & Oosthoek, J. H. P. (2014). Catastrophic ice lake collapse in Aram Chaos, Mars. *Icarus*, *236*, 104–121.

Rodriguez, J. A. P., Sasaki, S., Kuzmin, R. O., Dohm, J. M., Tanaka, K. L., Miyamoto, H., … Ferris, J. C. (2005). Outflow channel sources, reactivation, and chaos formation, Xanthe Terra, Mars. *Icarus*, *175*(1), 36–57.

Rotto, S., & Tanaka, K. L. (n.d.). *GEOLOGIC/GEOMORPHOLOGIC MAP OF THE CHRYSE PLANITIA REGION OF MARS*. Retrieved from https://pubs.usgs.gov/imap/2441/report.pdf

Scandone, R. (1990). Chaotic collapse of calderas. *Journal of Volcanology and Geothermal Research*, *42*(3), 285–302. https://doi.org/10.1016/0377-0273(90)90005-Z

Schmidt, G., Fueten, F., Stesky, R., Flahaut, J., & Hauber, E. (2018). Geology of Hebes Chasma, Mars: 1. Structure, Stratigraphy, and Mineralogy of the Interior Layered Deposits. *Journal of Geophysical Research: Planets*, *123*(11), 2893–2919. https://doi.org/10.1029/2018JE005658

Schultz, P. H., Schultz, R. A., & Rogers, J. (1982). The structure and evolution of ancient impact basins on Mars. *Journal of Geophysical Research: Solid Earth*, *87*(B12), 9803–9820.

Sowe, M, Wendt, L., McGuire, P. C., & Neukum, G. (2012). Hydrated minerals in the deposits of Aureum Chaos. *Icarus*, *218*(1), 406–419.

Sowe, Mariam, Stesky, R., Fueten, F., Sowe, M., Hauber, E., Jaumann, R., … Neukum, G. (2007). LAYERED DEPOSITS OF IANI CHAOS ON MARS Interior Layered Deposits in the Eastern Valles Marineris and Chaotic Terrains on Mars. *Lunar Planet. Sci.*, *XXXVIII*. https://doi.org/10.1029/2004JE002389

Tanaka, K. L., Robbins, S. J., Fortezzo, C. M., Skinner Jr, J. A., & Hare, T. M. (2014). The digital global geologic map of Mars: Chronostratigraphic ages, topographic and crater morphologic characteristics, and updated resurfacing history. *Planetary and Space Science*, *95*, 11–24.

Tanaka, K. L., Skinner, J. A., Hare, T. M., Kelley, M. S., Bleamaster Iii, L. F., Crown, D. A., … Williams, K. K. (n.d.). *Planetary Geologic Mapping Handbook-2009 The Geologic Mapping Subcommittee (GEMS) of the NASA Planetary Cartography and Geologic Mapping Working Group (PCGMWG)*. Retrieved from https://ntrs.nasa.gov/search.jsp?R=20100017213

Tange, O. (2011). GNU Parallel: The Command-Line Power Tool | USENIX. *The USENIX Magazine*, *3*(1), 42–47. Retrieved from https://www.usenix.org/publications/login/february-2011-volume-36-number-1/gnu-parallel-command-line-power-tool

Troll, V. R., Walter, T. R., & Schmincke, H.-U. (2002). Cyclic caldera collapse: Piston or piecemeal subsidence? Field and experimental evidence. *Geology*, *30*(2), 135–138.

Viviano-Beck, C. E., Seelos, F. P., Murchie, S. L., Kahn, E. G., Seelos, K. D., Taylor, H. W., … others. (2014). Revised CRISM spectral parameters and summary products based on the currently detected mineral diversity on Mars. *Journal of Geophysical Research: Planets*, *119*(6), 1403–1431.

Walter, T. R., & Troll, V. R. (2001). Formation of caldera periphery faults: an experimental study. *Bulletin of Volcanology*, *63*(2–3), 191.

Wilson, L., & Head III, J. W. (2002). Tharsis-radial graben systems as the surface manifestation of plume-related dike intrusion complexes: Models and implications. *Journal of Geophysical Research: Planets*, *107*(E8), 1.

Wyrick, D., Ferrill, D. A., Morris, A. P., Colton, S. L., & Sims, D. W. (2004). Distribution, morphology, and origins of Martian pit crater chains. *Journal of Geophysical Research: Planets*, *109*(E6).

Zegers, T. E., Oosthoek, J. H. P., Rossi, A. P., Blom, J. K., & Schumacher, S. (2010). Melt and collapse of buried water ice: An alternative hypothesis for the formation of chaotic terrains on Mars. *Earth and Planetary Science Letters*, *297*(3–4), 496–504.